

On the Anisotropy of the Stochastic Gravitational Wave Background from Sub-Horizon-Collapsed Primordial Black Hole Mergers

Stefano Profumo^{1,2} and Fengwei Yang³

¹*Department of Physics, University of California, Santa Cruz Santa Cruz, CA 95064, USA*

²*Santa Cruz Institute for Particle Physics, Santa Cruz, CA 95064, USA and*

³*Department of Physics and Astronomy, University of Utah, Salt Lake City, UT 84112, USA*

We study the properties of the stochastic gravitational wave background (SGWB) resulting from the mergers of primordial black holes (PBH) that formed from the collapse of sub-horizon regions in the early universe. We adopt a model-independent approach, where we parameterize the fraction f_H of the wavelength of the perturbation mode in units of the horizon radius when the patch starts to gravitationally collapse. Assuming a monochromatic spectrum of isocurvature perturbations and spherically-symmetric density perturbations, we investigate the isotropic SGWB energy density and angular power spectrum at various frequencies, PBH masses, and horizon size fractions. The key effect of sub-horizon formation is a change in the PBH mass function and formation redshift, which, in turn, affects gravitational wave (GW) observables. We find that sub-horizon PBH formation in general *enhances* the isotropic SGWB energy density and the absolute angular power spectrum. However, the quasi-monotonic increases in both quantities as f_H decreases cease when the chirp mass of the binary PBHs reaches a mass threshold determined by the frequency of observation; the isotropic SGWB energy density spectrum significantly drops above the corresponding cutoff frequency.

I. INTRODUCTION

The intriguing possibility that black holes form from large density fluctuations in the early universe instead of from the gravitational collapse of large astrophysical objects in the late universe was proposed long ago [1]. Such “primordial black holes” (PBHs) might be related to the cosmological dark matter [2], to the matter-antimatter asymmetry (see e.g. [3] and references therein), or both [4]; they could play a role in seeding supermassive black holes [5], or even explain part (or perhaps all) of the black hole-black hole mergers observed by gravitational wave (GW) interferometers [6]. While the direct detection of even a single black hole with a mass below the Tolman-Oppenheimer-Volkoff limit [7] would indicate the existence of PBHs (or of unexpected new physics [8]), other observables may point towards a non-astrophysical origin for black holes. For instance, the spin distribution expected from PBHs, whether produced in matter- or radiation-domination in the early universe, is expected to be markedly, or at least statistically significantly different than that expected for astrophysical black holes [9].

While no evidence for a stochastic background of GWs has been conclusively detected yet (see however [10]), there are several reasons to believe that it will soon be. A perfectly plausible source of such diffuse background are unresolved binary black hole mergers at all redshifts, including of PBHs [11]. Some information on the origin and production mechanism of the black holes whose binary mergers might contribute to the diffuse background of GWs may arise from spectral considerations [12]. Here, we rather focus on the use of the power spectrum of anisotropies of the stochastic background as a possible tell-tale signature of the production mechanism of the black holes (for previous studies see e.g. [13] and references therein).

Previous studies that focused on utilizing the anisotropy of the stochastic gravitational wave background (SGWB) as a metric to differentiate PBHs from astrophysical black holes include, for instance, Ref. [14] (see also Ref. [15] on how to utilize the isotropic SGWB to constrain the primordial origin of BH formation channel). Here, however, we take a different perspective, and aim at differentiating one particular aspect of PBH formation: the portion of the Hubble horizon that collapsed at formation. Generically, PBHs result from the collapse of patches of the early universe as large as the Hubble horizon at collapse, but depending on the formation mechanism the collapsing region can be significantly smaller. We therefore simply assume, here, in a model-agnostic way, that PBHs result from the collapse of a fraction $f_H < 1$ of the Hubble horizon only (we discuss expectations for f_H in different scenarios below), and study the impact of f_H on the anisotropy of the SGWB.

The remainder of this study is as follows: in the next section we discuss PBH formation from the collapse of curvature perturbations in the standard and in the presently investigated non-standard scenarios. Sec. III describes the calculation of the power spectrum of anisotropies of the SGWB, and presents our results. The final Sec. IV presents our discussion and conclusions.

II. PBH FORMATION FROM CURVATURE PERTURBATIONS

PBHs can form in the early universe as a result of the gravitational collapse of curvature perturbations $\zeta(x)$. The power spectrum of curvature perturbations, $P_\zeta(k)$, determines the width of the Gaussian distribution of matter overdensities $\delta\rho(x)/\rho(x) \equiv \delta(x)$. The distribution of matter overdensities then in turn determines the mass function of the resulting PBHs. According to the standard scenario, where a PBH is formed at the horizon re-entry time $t_H \sim 1/k_*$, with k_* the scale of the perturbation that collapses to form the PBH, the mass of the PBH is directly related, and proportional to, the Hubble mass – the mass enclosed at that time in a Hubble patch. The later the scale k_* reenters the horizon, the larger the PBH mass. Notably, and generically, however, *PBHs can be also formed at the sub-horizon scales*, and the formation time can be *much later* than t_H , modifying the relation between PBH mass and horizon mass. Here, we explore the implications of sub-horizon-forming PBHs for the anisotropy of the gravitational wave spectrum induced by the PBH merger.

A. The standard scenario for PBH formation

The horizon reentry time is defined by, in natural units,

$$t_H \equiv \frac{1}{k_*}, \quad (1)$$

where k_* is the scale of the over-density that will collapse to form a PBH, and where we denote the characteristic wavelength of the density perturbation as $\lambda_* \equiv 1/k_*$. The size of a Hubble patch at horizon re-entry is given by

$$r_H = t_H. \quad (2)$$

Thus, we can use Eq. (1) to relate the size of the Hubble patch at the horizon reentry time and the characteristic wavelength of the density perturbation,

$$\lambda_* = r_H. \quad (3)$$

Statistically-rare perturbations (such that one can neglect hierarchical random fields) are expected to be approximately spherically symmetric [16]. With the assumption that the perturbation is spherically symmetric, the amplitude of the smoothed density contrast $\bar{\delta}$ is related to the curvature perturbation, in radiation domination, as

$$\bar{\delta} = -\frac{2}{3}r_m\zeta'(r_m)(2 + r_m\zeta'(r_m)) = \delta_1 - \frac{3}{8}\delta_1^2, \quad (4)$$

where r_m is the smoothing scale, the prime is the derivative with respect to the radial coordinate, and δ_1 is the linear component of the $\bar{\delta}$, given by

$$\delta_1 = -\frac{4}{3}r_m\zeta'(r_m). \quad (5)$$

The distribution of δ_1 obeys a Gaussian probability distribution function (PDF):

$$\text{PDF}(\delta_1) = \frac{1}{\sqrt{2\pi\sigma^2}} \exp\left(-\frac{\delta_1^2}{2\sigma^2}\right), \quad (6)$$

where the variance σ_0^2 characterizes the width of the Gaussian PDF, and it is obtained from the zeroth moment of the power spectrum of δ_1 . The j -th moments of the power spectrum P_{δ_1} are given by

$$\sigma_j^2 = \int_0^\infty \frac{dk}{k} P_{\delta_1}(k, r_m) \left(\frac{k}{aH}\right)^{2j}. \quad (7)$$

The variance is

$$\sigma_0^2 = \langle \delta_1^2 \rangle = \int_0^\infty \frac{dk}{k} P_{\delta_1}(k, r_m) = \frac{16}{81} \int_0^\infty \frac{dk}{k} (kr_m)^4 \tilde{W}^2(k, r_m) T^2(k, r_m) P_\zeta(k), \quad (8)$$

where we choose a Dirac- δ peak power spectrum of the curvature perturbation $P_\zeta(k) = A_s \delta\left(\ln \frac{k}{k_*}\right) + A_b$ ($A_s \gg A_b$), A_s and A_b are the amplitudes of the short-wavelength mode and background mode, respectively, r_m is the smoothing scale that determines how to choose the spatial volume to average the overdensity peak,

$$\tilde{W}(k, r_m) = 3 \frac{\sin(kr_m) - kr_m \cos(kr_m)}{(kr_m)^3} \quad (9)$$

is the Fourier transform of the top-hat window function with the time-dependent smoothing scale r_m , and

$$T(k, r_m) = 3 \frac{\sin(kr_m/\sqrt{3}) - kr_m/\sqrt{3} \cos(kr_m/\sqrt{3})}{(kr_m/\sqrt{3})^3} \quad (10)$$

is the linear transfer function. In the literature [17], it is common to choose the smoothing scale to be the Hubble scale, i.e., $r_m(z) = r_H = (aH)^{-1}$.

When the smoothed density contrast $\bar{\delta}$ is greater than the critical threshold value δ_c , a PBH is formed, with a mass closely related to the modeling of the gravitational collapse,

$$M_{\text{PBH}} = \mathcal{K}(\bar{\delta} - \delta_c)^\gamma M_H, \quad (11)$$

where M_H is the horizon mass at the formation time of PBH, $\mathcal{K} = 4$ accounts for most of the shape of the density contract, $\gamma = 0.36$ is the critical exponent dependent on the equation of state of the universe and here is evaluated in the radiation-dominated era [17], and $\delta_c = 0.51$ is chosen for a typical profile shape of the density perturbation and a real-space top-hat window function at the horizon reentry time [18, 19]. Given the above PBH formation model, the distribution of the Gaussian random field δ_1 thus determines the abundance and mass function of the resulting PBHs. By inverting Eq. (11) and combining with Eq. (4), one can obtain the value of δ_1 corresponding to a given PBH mass M_{PBH} ,

$$\delta_1(M_{\text{PBH}}) = \frac{2}{3} \left(2 - \sqrt{4 - 6\delta_c - 6 \left(\frac{M_{\text{PBH}}}{\mathcal{K}M_H} \right)^{1/\gamma}} \right). \quad (12)$$

The initial abundance of PBHs is usually described by the energy density fraction of PBHs in the universe at a single formation time,

$$\beta = \int_{\mu_c}^{\mu_{\text{max}}} d\mu \frac{M_{\text{PBH}}(\mu)}{M_H} n_{\text{peak}}(\mu), \quad (13)$$

where $\mu \equiv \delta_1/\sigma_0$, $\mu \in [\mu_c, \mu_{\text{max}}]$, $\mu_c = \delta_{c,1}/\sigma_0$, $\mu_{\text{max}} = \delta_{1,\text{max}}/\sigma_0 = 4/(3\sigma_0)$, makes the gravitational collapse happen, $\delta_{c,1} = \frac{4}{3} \left(1 - \sqrt{1 - \frac{3}{2}\delta_c} \right)$ is the critical value for gravitational collapse of δ_1 , $n_{\text{peak}} = \frac{1}{4\pi^2} \left(\frac{\sigma_1}{\sigma_0} \right)^3 \mu^3 \exp\left(-\frac{\mu^2}{2}\right)$ is the number density of over-density peaks in a comoving volume [16].

The mass function is defined as

$$\Psi(M_{\text{PBH}}) = \frac{1}{f_{\text{PBH}}} \frac{df_{\text{PBH}}}{dM_{\text{PBH}}}, \quad (14)$$

such that $\int \Psi(M_{\text{PBH}}) dM_{\text{PBH}} = 1$, where $f_{\text{PBH}} \equiv \Omega_{\text{PBH}}/\Omega_{\text{DM}}$ is the fraction of the present dark matter (DM) energy density stored in PBHs. The fraction f_{PBH} can be calculated from β by integrating the contributions from PBHs formed across the history of the universe until the time of matter-radiation equality,

$$f_{\text{PBH}} = \frac{1}{\Omega_{\text{DM}}} \int_{M_{H,\text{min}}}^{M_{H,\text{max}}} d(\ln M_H) \left(\frac{M_{H,\text{eq}}}{M_H} \right)^{1/2} \beta(M_H), \quad (15)$$

where $M_{H,\text{eq}} = \frac{4\pi}{3} 2\rho_{\text{eq}} H_{\text{eq}}^{-3} \approx 2.8 \times 10^{17} M_\odot$ is the approximate horizon mass at the matter-radiation equality. Assuming a Dirac- δ form for the power spectrum of the curvature perturbation and assuming as a result that all PBHs form at a single time, the mass function is given by

$$\Psi(M_{\text{PBH}}) = \frac{1}{\beta} \frac{d\beta}{dM_{\text{PBH}}}. \quad (16)$$

Here is the derivation. First, we relate β , the abundance of PBHs at a single formation time, to Ω_{PBH} , the energy density parameter of PBHs observed today:

$$\beta = \frac{\rho_{\text{PBH}}}{\rho_r} = \frac{\rho_{\text{PBH}}}{\rho_{c,0}} \frac{\rho_{c,0}}{\rho_r} = \frac{\rho_{\text{PBH},0} \left(\frac{a_0}{a}\right)^3}{\rho_{c,0}} \frac{\rho_{c,0}}{\rho_{r,0} \left(\frac{a_0}{a}\right)^4 \left(\frac{g_0}{g}\right)^{1/3}} = \frac{\Omega_{\text{PBH}}}{\Omega_r} \left(\frac{a}{a_0}\right) \left(\frac{g}{g_0}\right)^{1/3}, \quad (17)$$

where Ω_r is the energy density parameter of radiation observed today, a is the scalar factor, $a_0 = 1$ is the scalar factor today, g and g_0 are the degree of freedom of the relativistic species at the time of a and a_0 respectively. Therefore, the energy density fraction of PBHs in terms of DM is given by a simplified expression instead of the integral in Eq. (15),

$$f_{\text{PBH}} = \frac{\Omega_{\text{PBH}}}{\Omega_{\text{DM}}} = \frac{\Omega_r}{\Omega_{\text{DM}}} \frac{1}{a} \left(\frac{g_0}{g}\right)^{1/3} \beta. \quad (18)$$

Let $\psi(x) = \Psi \times M_H$ be a dimensionless mass function:

$$\psi(x) = \frac{1}{4\pi^2 \beta \sigma_0} x \left(\frac{\sigma_1}{\sigma_0}\right)^3 \left(\frac{\delta_1(x)}{\sigma_0}\right)^3 \exp\left(-\frac{\delta_1^2(x)}{2\sigma_0^2}\right) \frac{\sqrt{2}(x/\mathcal{K})^{1/\gamma-1}}{\gamma \mathcal{K} \sqrt{2-3\delta_c-3(x/\mathcal{K})^{1/\gamma}}}, \quad (19)$$

where $x \equiv \frac{M_{\text{PBH}}}{M_H}$ is the ratio between PBH mass and horizon mass. The normalization of the dimensionless mass function becomes $\int \psi(x) dx = 1$, and the PBH-mass-to-horizon-mass ratio x ranges from 0 to 2.05, where the upper limit is coming from the that Eq. (4) has a maximum value $\bar{\delta} = \frac{2}{3}$ such that

$$M_{\text{PBH,max}} = \mathcal{K} \left(\frac{2}{3} - \delta_c\right)^\gamma M_H = 2.05 M_H, \quad (20)$$

where the second identity is obtained by substituting the parameters of the PBH formation model used in this paper.

B. Sub-horizon PBH formation

Generically, a PBH can form from the collapse of a density perturbation of λ_* smaller than the size of the horizon by a factor f_H ,

$$\lambda_* = f_H \times r'_H, \quad (21)$$

where we use the symbol r'_H to indicate the Hubble patch where the PBH is formed. For example, Ref. [20] considers $f_H = 1/4$. Several example formation mechanisms with $f_H \lesssim 1$ and/or with $f_H \ll 1$ have been proposed and discussed in detail in the literature. For instance, Ref. [21] considers PBH production from the collapse of scalar field lumps (Q-balls or oscillons) that can potentially temporarily dominate the energy density of the universe leading to efficient PBH formation; the typical size of the lumps (formed, here, not because of gravitational instability, but rather due to self-interactions) is predicted, from numerical simulations, to be a fraction $f_Q \sim 10^{-2} - 10^{-1}$ of the horizon size. Bubble collision upon spontaneous symmetry breaking and a first-order phase transition also generically seed sub-horizon density perturbations leading to collapse into black holes with mass much smaller than the horizon mass (see e.g. [22]). Similarly, cosmic string loops lead to sub-horizon mass PBH, depending on the string tension [23, 24]. Ref. [25] entertains a more speculative possibility of multigravitino Bogomol'nyi-Prasad-Sommerfield (BPS) states that if sufficiently large could collapse into black holes whose mass is entirely unrelated to the horizon mass. A somewhat less speculative possibility is the collapse of Fermi balls consisting of massive fermions trapped into regions of false vacuum in a first-order phase transition [26]. Other similar possibilities include the formation of PBH from long-range scalar forces and scalar radiative cooling [27], and a late-phase transition in a strongly interacting fermion-scalar fluid [28]. Finally, the collapse of neutron stars in the very late universe, possibly triggered by the accumulation of dark matter in the neutron star core, can also lead to the formation of black holes with masses much smaller than the horizon mass [8, 29].

For $f_H < 1$, one has $r'_H = r_H / f_H > r_H$, i.e., the Hubble patch where the PBH is formed is greater than the one in the standard scenario, and thus the formation time is later than the one in the standard scenario, $t'_H > t_H$. Assuming PBHs formed in the early universe, during radiation domination, the formation redshift can be related to the one in the standard scenario by the following equation:

$$\frac{z'_{\text{form}}}{z_{\text{form}}} = f_H. \quad (22)$$

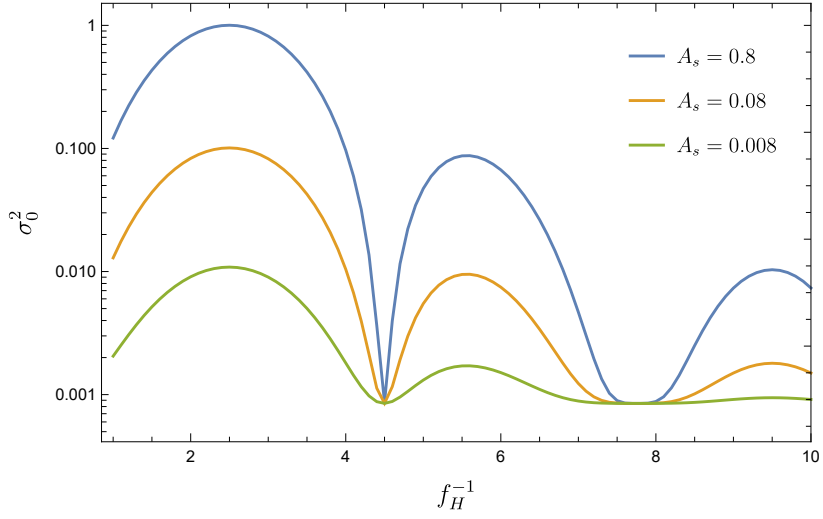


FIG. 1. The variance σ_0^2 of the over-density distribution as a function of $1/f_H$, for different amplitudes of the short-wavelength perturbation mode $A_s = 0.8$ (blue), 0.08 (orange), 0.008 (green), at a fixed value for the amplitude of the background mode $A_b = 8 \times 10^{-4}$.

In the sub-horizon formation scenario, $r_m(z)$ in Eq. (8) is evaluated at time z'_{form} instead of z_{form} , such that $k_* r_m (= f_H^{-1}) \neq 1$. There is one subtlety for the smoothing scale of the top-hat window function. In the standard case, there is only one density contrast peak in one Hubble patch, so choosing $r_m = r_H$ is reasonable. However, in the sub-horizon formation case, there are $\lfloor f_H^{-1} \rfloor$ density contrast peaks, but we still choose $r_m = r_H$ as the smoothing scale. We comment later on the impact of choosing different smoothing radii and how our results depend on the choice of r_m .

Figure 1 shows σ_0^2 as a function of the inverse of the horizon size fraction f_H^{-1} for different values of A_s with a fixed value of $A_b = 8 \times 10^{-4}$. For a given A_s , σ_0^2 increases monotonically before reaching its maximum at $f_H^{-1} \sim 2.5$, and it rapidly drops until it reaches its minimum at $f_H^{-1} \sim 4.5$. The behavior of σ_0^2 is quasi-periodic with respect to f_H^{-1} because the window function and transfer function in Eq. (8), containing $\sin(k_* r_m) = \sin(f_H^{-1})$ and $\cos(k_* r_m) = \cos(f_H^{-1})$, are periodic but with a suppressed amplitude at larger f_H^{-1} . Figure 1 additionally illustrates how the value of σ_0^2 decreases globally for a smaller value of A_s , because σ_0^2 characterizes the auto-correlation of the overdensity whose amplitude is determined by the amplitude of the curvature perturbation. We stress that the non-linear dependence of the value of σ_0^2 on A_s at some values of f_H stems from the fact that the ratio A_s/A_b is not a constant. If A_s/A_b were a constant, σ_0^2 would linearly depend on A_s , which can be directly derived from Eq. (8). Starting from the Sec. III, for simplicity, we choose $A_b = 0$, and the j -th order moments are simplified to be

$$\sigma_j^2 = 432 A_s f_H^{8-2j} (\sin(f_H^{-1}) - f_H^{-1} \cos(f_H^{-1}))^2 \left(\sin(f_H^{-1}/\sqrt{3}) - f_H^{-1}/\sqrt{3} \cos(f_H^{-1}/\sqrt{3}) \right)^2. \quad (23)$$

We note that the above dependence on A_s and f_H brings a degeneracy of A_s when fixing f_{PBH} and f_H . This is because f_{PBH} is proportional to β , which, in turn, is only determined by σ_0^2 and σ_1^2 (see Eq. (13)); specifically, β has an exponential dependence on σ_0^2 , and a power-law dependence on σ_1^2 . This results in f_{PBH} being approximately fixed by a given choice of σ_0^2 . However, Eq. (23) can have multiple roots for A_s when fixing σ_0^2 and f_H , which can also be appreciated by imagining a horizontal line in Figure 1 and noting how it would intersect with curves of different colors from a large σ_0^2 value to a smaller value. Therefore, A_s has multiple values for given f_{PBH} and f_H . Also, due to the quasi-periodic behavior of σ_0^2 versus f_H , one has the freedom to pick A_s such that f_{PBH} is sufficiently small at a given f_H . In the calculation of Sec. III, we fix $f_{\text{PBH}} = 0.01$ and choose the *smallest value* of A_s for each f_H . Eq. (23) also manifests choosing different smoothing scales r_m will change the value of σ_0^2 and σ_1^2 . For the choice of $r_m = r_H$, $k_* r_m = f_H^{-1}$, while in general, one can choose $f_H r_H \leq r_m \leq r_H$, i.e., $1 \leq k_* r_m \leq f_H^{-1}$.

Figure 2 shows (on a linear (left) and logarithmic (right) scale) the mass function of Eq. (19) for different values of the variance σ^2 induced by $A_s = 0.8$, 0.08 , and 0.008 , again at fixed $A_b = 8 \times 10^{-4}$. The log-log plots (Figure 2 right panels) illustrate how the mass function exhibits a power-law behavior when the normalized PBH mass $x < x_0$, where x_0 is the point at which the mass function reaches its local maximum. However, we note that for $A_s = 0.8$, $f_H = 1/2$ and $1/3$, the mass function does not have a local maximum, but, rather, it monotonically increases as a function of the PBH mass, while for the other it is exponentially suppressed when $x > x_0$. This behavior can be

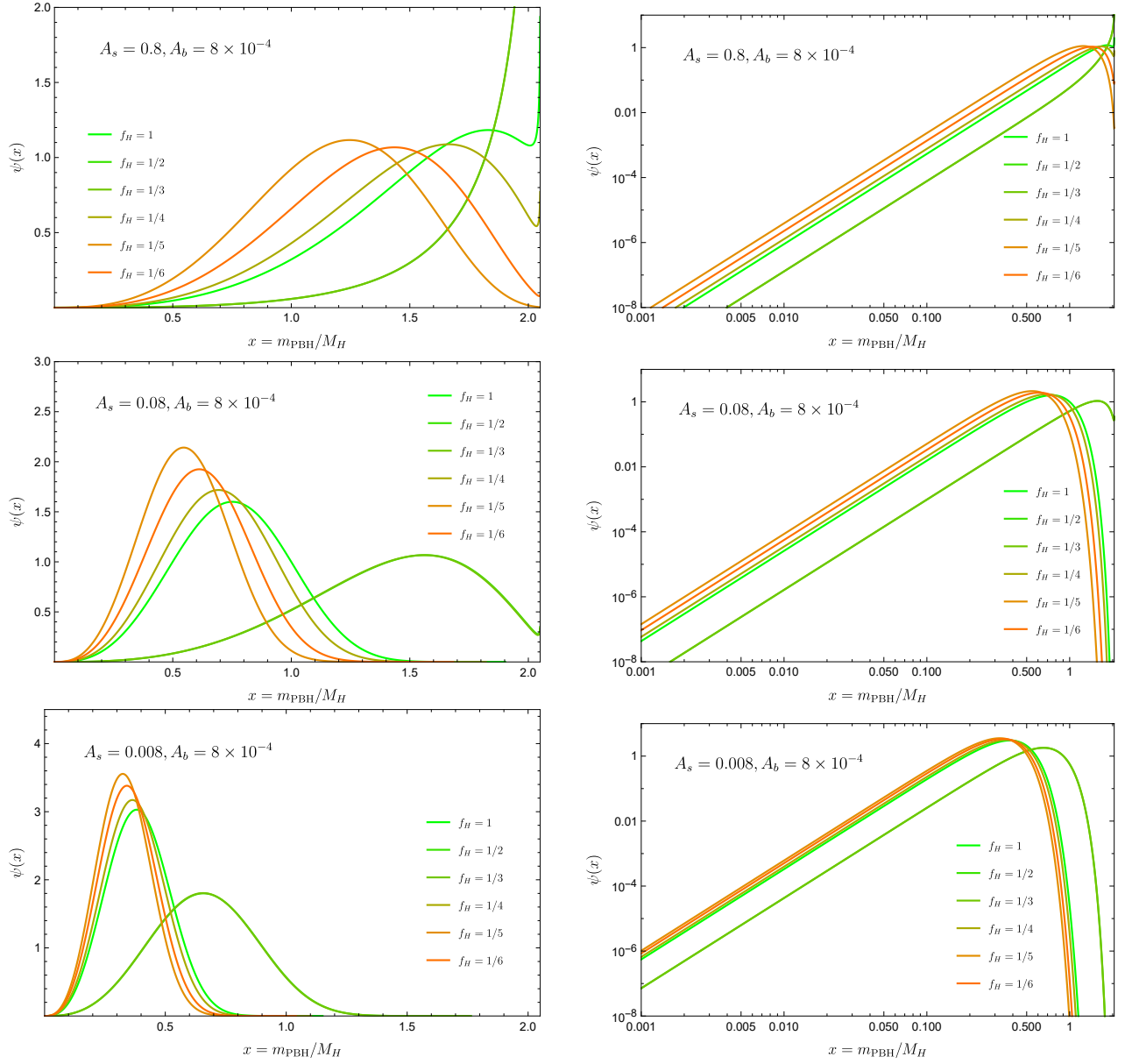


FIG. 2. The mass function of PBH for different values of f_H , for $A_s = 0.8$ (top panels), 0.08 (middle panels) and 0.008 (bottom panels) with $A_b = 8 \times 10^{-4}$ in all cases. Left column: linear-linear scale. Right column: log-log scale.

explained as follows: the exponential function $\exp\left(-\frac{\delta_1^2(x)}{2\sigma_0^2}\right)$ in Eq. (19) decreases monotonically as x increases for a given σ_0^2 but with a different decreasing rate which depends sensitively on the value of σ_0^2 . For $f_H^{-1} = 2$ or 3 when $A_s = 0.8$, the value of $\sigma_0^2 \sim 0.8$, which is almost an order of magnitude larger than σ_0^2 at other f_H^{-1} , such that the decrease in $\exp\left(-\frac{\delta_1^2(x)}{2\sigma_0^2}\right)$ is counter-balanced by the increase in the remaining x -dependent part in Eq. (19). For other f_H^{-1} values, since the corresponding value of σ_0^2 is small (~ 0.1), the behavior of the mass function at large x is instead mainly determined by the exponential suppression originated from $\exp\left(-\frac{\delta_1^2(x)}{2\sigma_0^2}\right)$.

We also investigate the mass function at a very small f_H , i.e., very large f_H^{-1} , ranging from $f_H^{-1} \in [10, 5000]$ in Figure 3 which shows the mass function at $f_H \ll 0.1$ in the left panel and the ratio of mass functions normalized by the “standard” mass function corresponding to $f_H = 1$ in the right panel. We note that for $f_H \leq 1/30$, the mass functions for different values of f_H are self-similar. The reason is that the mass function $\psi(x)$ only depends on the value of $\sigma_0^2 = \sigma_0^2(f_H)$ and when $f_H \leq 1/30$, $\sigma_0^2 \approx 0.00085 \sim A_b$ does not significantly change.

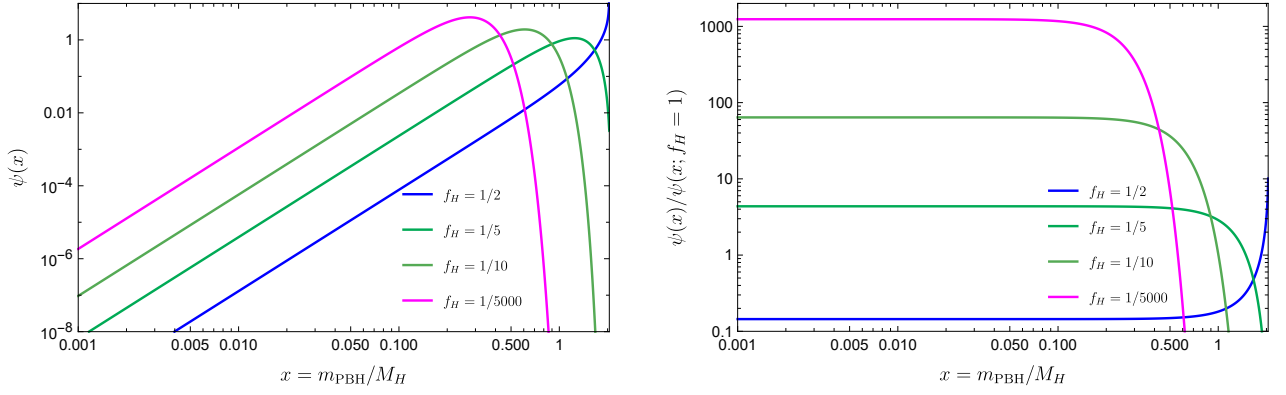


FIG. 3. The mass function (left) and the one normalized by the mass function of $f_H = 1$ (right) for $f_H \leq 0.1$, $A_s = 0.8$, and $A_b = 8 \times 10^{-4}$.

III. ANISOTROPIC SGWB ENERGY DENSITY POWER SPECTRUM

If two PBHs, separated by a distance x , have an energy density $4M/(3\pi x^3)$ larger than the cosmic radiation energy density ρ_r (since we suppose PBHs are formed deep in the radiation era, radiation is the dominant component of the universe), they decouple from the Hubble flow and become a gravitationally bound binary system. PBH binaries then radiate GWs during the inspiral, merger, and ring-down phases [30]. The incoherent superposition of the unresolved GWs emitted by such PBH binaries contributes to SGWBs across several orders of magnitude in frequency, which advanced LIGO or LISA can detect in the near future [31]. The SGWB produced by PBH binaries has both an isotropic and an anisotropic component: while only spectral information can be extracted from the former, we focus on the latter, the anisotropic component in seeking a way to ascertain whether the PBH formation history corresponds to a standard horizon-size collapse, or to the aforementioned sub-horizon-collapse scenarios. As such, *the scope of the present study is to seek for distinguishable features of PBH binary mergers in the standard versus sub-horizon formation scenarios by studying the anisotropic component.*

As customary [32], we define as the isotropic SGWB energy density spectrum the dimensionless quantity

$$\bar{\Omega}_{\text{gw}}(\nu) \equiv \frac{\nu}{\rho_c} \frac{d\rho_{\text{gw}}}{d\nu}, \quad (24)$$

where ρ_c is the critical energy density of the universe and ρ_{gw} is the SGWB energy density. In a more general situation where the SGWB has directional dependence, the definition is supplemented by

$$\Omega_{\text{gw}}(\nu, \mathbf{n}) \equiv \frac{1}{\rho_c} \frac{d^3 \rho_{\text{gw}}(\nu, \mathbf{n})}{d \ln \nu d^2 \mathbf{n}} = \frac{\bar{\Omega}_{\text{gw}}}{4\pi} (1 + \delta(\nu, \mathbf{n})), \quad (25)$$

where $\rho(\nu, \mathbf{n})$ is the SGWB energy density at frequency ν along the line-of-sight direction \mathbf{n} , $\delta(\nu, \mathbf{n})$ denotes the anisotropic fluctuations.

The isotropic component $\bar{\Omega}_{\text{gw}}(\nu)$ produced by PBH binary mergers is given by the following integral:

$$\bar{\Omega}_{\text{gw}}(\nu) = \frac{\nu}{\rho_c} \int_0^{z_*} \frac{dz}{(1+z)H(z)} \int d\Theta_s \mathcal{R}(\Theta_s, z) \frac{dE}{d\nu}(\nu_s, \Theta_s), \quad (26)$$

where z is redshift, z_* corresponds to the formation time of PBHs, $H(z) = H_0 \sqrt{\Omega_r(1+z)^4 + \Omega_m(1+z)^3 + \Omega_\Lambda}$ is the Hubble parameter, \mathcal{R} is the merger rate of PBH binaries, $dE/d\nu(\nu_s, \Theta)$ is the energy spectrum at source frequency $\nu_s = \nu \times (1+z)$, with source parameters Θ_s describing masses, eccentricity, and so on. The energy spectrum used in our calculation is derived from the inspiral-merger-ringdown waveforms for non-spinning PBH binaries given e.g. in Ref. [33, 34]. Figure 4 shows the isotropic SGWB energy density $\bar{\Omega}_{\text{gw}}(\nu; f_H)$ as a function of f_H^{-1} at different observed frequencies and different $M_{\text{PBH, max}}$, in which we use the merger rate \mathcal{R} (see Eq. (31)) that is to be introduced later to take into account the effect of the sub-horizon formation.

The cross-correlation of the anisotropies in SGWB between two different directions \mathbf{n} and \mathbf{n}' , $\langle \delta(\nu, \mathbf{n}) \delta(\nu, \mathbf{n}') \rangle$, describes the amplitude of the statistical fluctuation at a certain angular scale $\mathbf{n} \cdot \mathbf{n}'$. By decomposing it in a spherical harmonic basis, we have

$$\langle \delta(\nu, \mathbf{n}) \delta(\nu, \mathbf{n}') \rangle = \sum_l \frac{2l+1}{2\pi} C_l P_l(\mathbf{n} \cdot \mathbf{n}'), \quad (27)$$

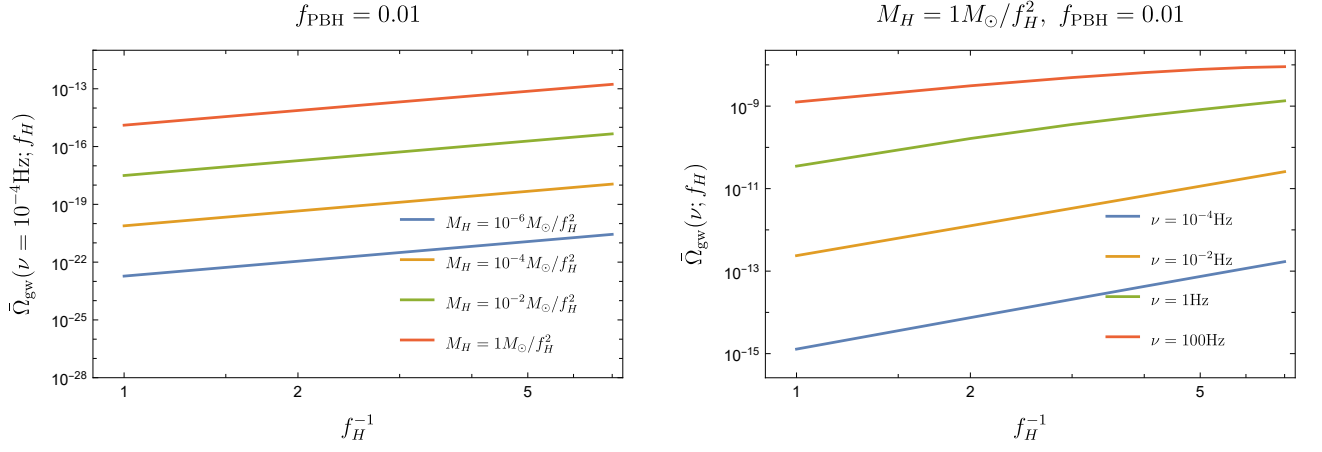


FIG. 4. The isotropic component of the SGWB energy spectrum at $\nu = 10^{-4}\text{Hz}$ with different $M_{\text{PBH,max}} = M_H = 10^{-6}M_\odot/f_H^2$, $10^{-4}M_\odot/f_H^2$, $10^{-2}M_\odot/f_H^2$, and $1M_\odot/f_H^2$ (left), and the standard case at $M_{\text{PBH,max}} = 1M_\odot/f_H^2$, for different observed frequencies $\nu = 10^{-4}\text{Hz}$, 10^{-2}Hz , 1Hz , and 100Hz (right). We fix $f_{\text{PBH}} = 0.05$.

and the dimensionless angular power spectrum is given by

$$C_l(\nu) \equiv \frac{2}{\pi} \int d\ln k k^3 |\delta_l(k, \nu)|^2, \quad (28)$$

where $\delta_l(k, \nu)$ is the Fourier transforms of the spatial anisotropies $\delta(\nu, \mathbf{n})$, and are given by [35],

$$\begin{aligned} \delta_l(\nu, k) = & \frac{\nu}{\Omega_{\text{gw}}(\nu)\rho_c} \int_{\eta_*}^{\eta_0} d\eta \mathcal{L}(\eta, \nu_s) \\ & \times \left\{ [4\Psi_k(\eta) + 4\Pi_k(\eta) + b\delta_{m,k}(\eta)] j_l(k\Delta\eta) - 2kv_k(\eta)j'_l(k\Delta\eta) - 6 \int_{\eta_0}^{\eta} d\eta' \dot{\Psi}_k(\eta') j_l(k\Delta\eta') \right. \\ & \left. + \frac{\partial \ln(dE/d\nu_s)}{\partial \ln \nu_s} \left[-\Psi_k(\eta) j_l(k\Delta\eta) - \Pi_k(\eta) j_l(k\Delta\eta) + kv_k(\eta) j'_l(k\Delta\eta) + 2 \int_{\eta_0}^{\eta} d\eta' \Psi_k(\eta') j_l(k\Delta\eta') \right] \right\}, \quad (29) \end{aligned}$$

where $\mathcal{L}(\eta, \nu_s) = a(\eta) \int d\Theta_s \mathcal{R}(\Theta_s, z(\eta)) \frac{dE}{d\nu}(\nu_s, \Theta_s)$ is the GW luminosity of the PBH binary merger, the galaxy bias $b = 1$ for PBH, $\Psi_k \approx \phi_k$ and $\Pi_k = 0$ are two scalar gravitational potentials, $\delta_{m,k}$ is the matter density contrast, v_k is the velocity of matter, the dot represents the derivative with respect to conformal time η . The corresponding transfer functions are calculated numerically by solving the linearized cosmological perturbation equations in CLASS, and the primordial scalar fluctuation power spectrum is $P_s(k) = \mathcal{A}_s^2 k^{-3} (k/k_0)^{n_s-1}$, where $\mathcal{A}_s = 2.215 \times 10^{-9}$, $n_s = 0.96$, and $k_0 = 0.05\text{Mpc}^{-1}$ are chosen from the Planck 2018 results [36], and j_l is the spherical Bessel function.

By comparing the numerical results of δ_l in Eq. (29) with or without including the v_k 's and ϕ_k 's terms, we find that only the term with the matter density contrast δ_m is dominant in the calculation, so it can be approximated by

$$\delta_l(\nu, k) = \frac{\nu}{\Omega_{\text{gw}}(\nu)\rho_c} \int_{\eta_*}^{\eta_0} d\eta \mathcal{L}(\eta, \nu_s) \delta_{m,k}(\eta) j_l(k\Delta\eta). \quad (30)$$

We assume that the merger rate of PBH is given by the functional form [37],

$$\mathcal{R}(\Theta_s, \tau) = 1.6 \times 10^6 \text{Gpc}^{-3} \text{yr}^{-1} f_{\text{PBH}}^{53/37} \eta(m_1, m_2)^{-34/37} \left(\frac{m_1 + m_2}{M_\odot} \right)^{-32/37} \left(\frac{\tau}{t_0} \right)^{-34/37} \Psi(m_1) \Psi(m_2) S(f_{\text{PBH}}), \quad (31)$$

where f_{PBH} (not to be confused with f_H) is the fraction of PBH at the present time t_0 , $\eta(m_1, m_2) = m_1 m_2 / (m_1 + m_2)^2$ is the symmetric factor for the binary, $\Psi = \Psi(m; f_H)$ is the mass function which is defined in the previous section, and $S(f_{\text{PBH}}) = \left(\frac{5f_{\text{PBH}}^2}{6\sigma_M^2} \right)^{21/74} U\left(\frac{21}{74}, \frac{1}{2}, \frac{5f_{\text{PBH}}^2}{6\sigma_M^2}\right)$ is the suppression factor with U the confluent hypergeometric function. Notice that we assume that the form of the merger rate is unchanged in the sub-horizon formation scenario, i.e., $\Psi(m; f_H)$ can be evaluated when $f_H < 1$, which is strongly physically motivated.

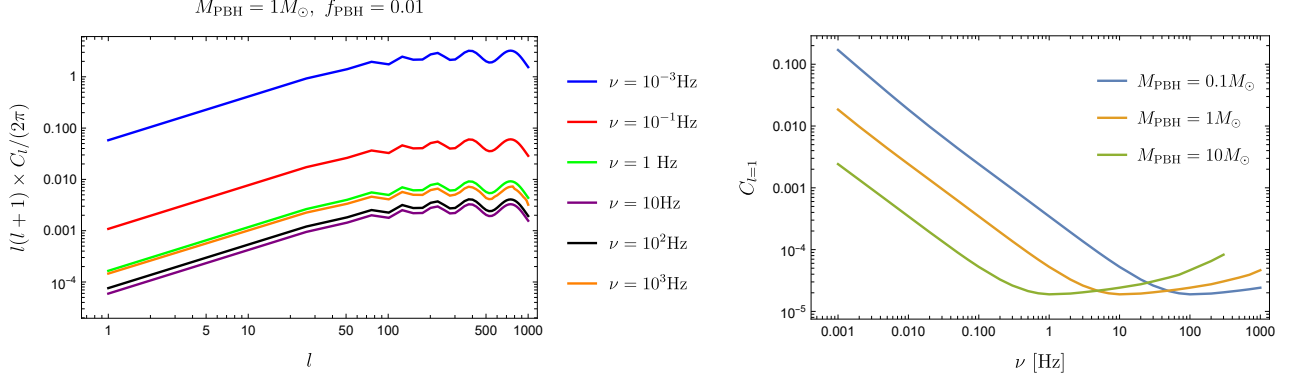


FIG. 5. The angular power spectrum at multiple frequencies at a fixed PBH mass $M_{\text{PBH}} = 1M_\odot$ (left). The relative amplitude of angular power spectrum at $l = 1$ as a function of frequency ν for three different PBH masses $M_{\text{PBH}} = 0.1, 1, 10 M_\odot$ (right).

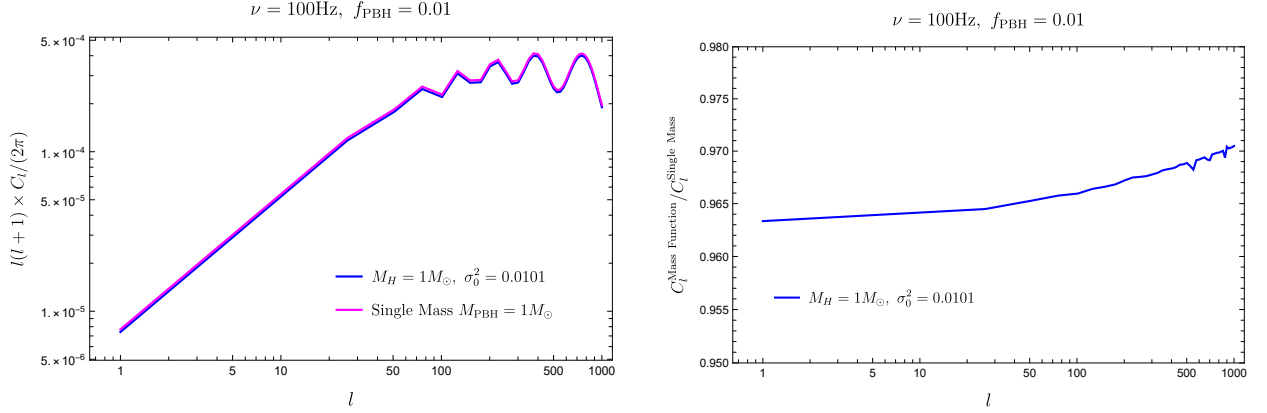


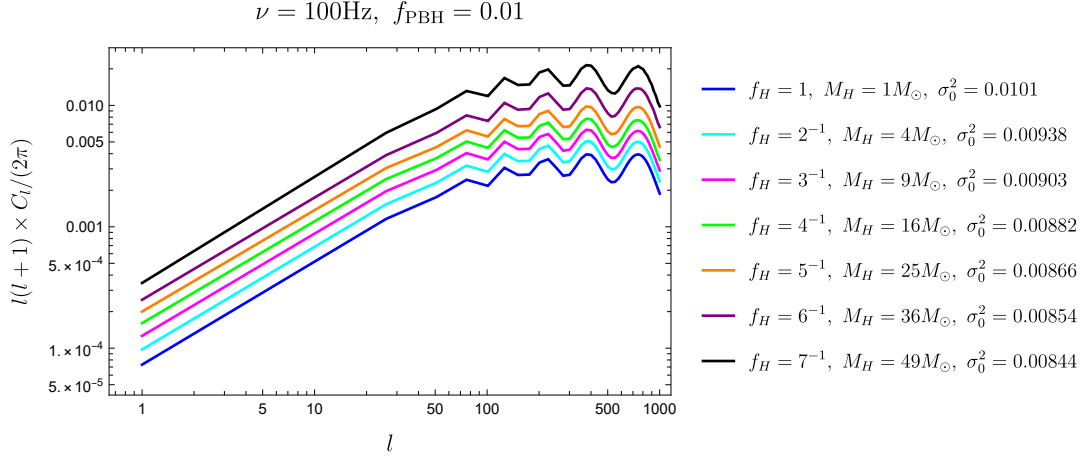
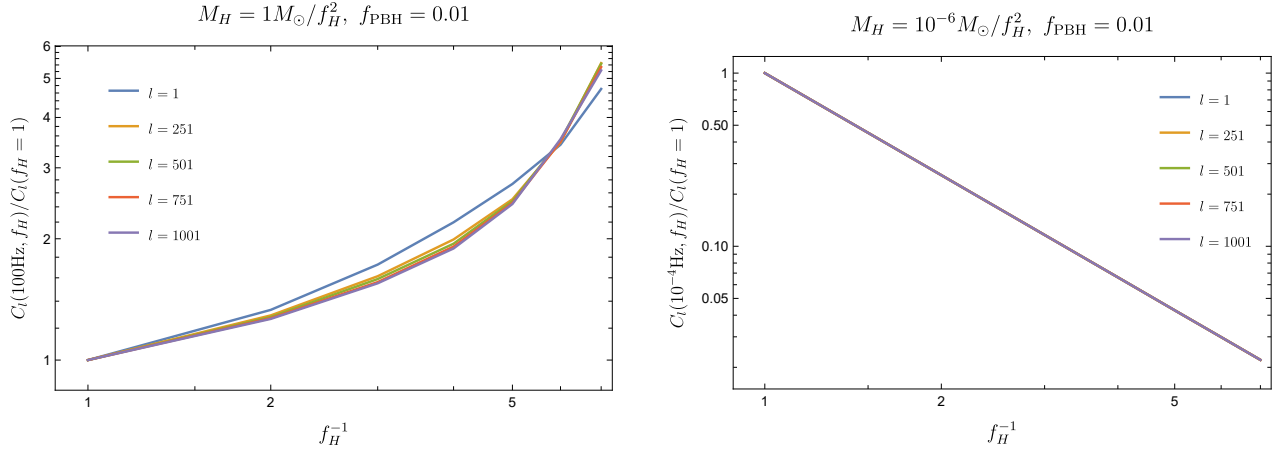
FIG. 6. The angular power spectrum C_l at 100 Hz with PBH masses given by a mass function ($f_H = 1$ and $\sigma_0^2 = 0.0101$ such that $f_{\text{PBH}} = 0.01$) and by a fixed PBH mass $M_{\text{PBH}} = 1M_\odot$ (left). The ratio of C_l between the mass function cases and the single mass case (right).

Figure 5, left, shows the typical angular power spectrum of the SGWB anisotropic component for PBH binary mergers in the standard scenario. We choose a Dirac- δ mass function in the merger rate such that $M_{\text{PBH}} = M_H = 1M_\odot$, and thus PBHs are formed deep in the radiation-dominated era with $z_{\text{form}} = 1.62 \times 10^{12}$. The right panel shows the frequency dependence of the $l = 1$ dipole as a function of frequency for various choices of the PBH mass $M_{\text{PBH}} = 0.1, 1, 10 M_\odot$, illustrating how larger chirp masses, $M_c = 2^{-1/5} M_{\text{PBH}}$ for a binary PBH with the same mass, induce a lower dipole amplitude at low frequency and a larger amplitude at higher frequencies, as expected.

In Figure 6 we compare the angular power spectrum obtained before to that corresponding to a mass function arising from a value of σ_0^2 such that $f_{\text{PBH}} = 0.01$ at a frequency $\nu = 100\text{Hz}$ (the right plot shows the ratio of the curves at a given σ_0^2 to the standard case). There are no large deviations between the angular power spectra besides an overall amplitude shift due to the different weighting on the PBH mass function. The single mass case has a Dirac- δ peak mass function, while the other has a mass function determined by σ_0^2 .

f_H^{-1}	1	1.2	1.4	1.6	1.8	2	3	4	5	6	7
$\bar{\Omega}_{\text{gw}}/10^{-9}$	1.26	1.61	1.98	2.36	2.73	3.11	4.93	6.49	7.77	8.63	9.04
σ_0^2	0.0101	0.00988	0.00972	0.00959	0.00948	0.00938	0.00903	0.00882	0.00866	0.00854	0.00844
σ_1^2	0.0101	0.0142	0.0191	0.0245	0.0307	0.0375	0.0813	0.141	0.217	0.307	0.413
A_s	0.0668	0.0357	0.0219	0.0150	0.0112	0.00913	0.00885	0.0736	0.149	0.103	1.76

TABLE I. Values of the isotropic SGWB energy density $\bar{\Omega}_{\text{gw}}$ at 100 Hz, the zeroth order and first order width, and the amplitude of Dirac- δ curvature power spectrum for a fixed f_{PBH} and different f_H^{-1} .

FIG. 7. The angular power spectrum at 100 Hz for different f_H .FIG. 8. The angular power spectra of $l = 1, 251, 501, 751$, and 1001 as a function of f_H^{-1} , normalized by $C_l(f_H = 1)$ for the corresponding l , for $\{1M_\odot, 100\text{Hz}\}$ (left) and $\{10^{-6}M_\odot, 10^{-4}\text{Hz}\}$ (right).

To study the effects of $f_H \neq 1$, we study the SGWB from an f_H -dependent mass function $\Psi(m; f_H)$ to investigate the effect of sub-horizon formation on the angular power spectrum. Figure 7 shows the angular power spectrum at 100 Hz for $f_H = m^{-1}$, $1 \leq m \leq 7$ and $m \in \mathbb{N}$. The amplitude of the angular power spectrum increases as f_H^{-1} increases when $f_H^{-1} \in [1, 6]$, but slightly decreases when $f_H^{-1} \in (6, 7]$. Table I summarizes the isotropic SGWB energy density values, σ_0^2 , σ_1^2 , and A_s required to match a given $f_{\text{PBH}} = 0.01$ for different f_H (including some fractional values of m).

We are also interested in the effect of sub-horizon formation on the angular power spectrum C_l at different multipole l 's. We show the normalized C_l (i.e. the ratio $C_l(f_H)/C_l(f_H = 1)$) in Figure 8, for different parameter sets $\{M_H f_H^2, \nu\}$, in which the first parameter sets the horizon mass when PBHs form for different f_H and the second parameter is the observed frequency of the angular power spectrum. The left panel employs $\{1M_\odot, 100\text{Hz}\}$ while the right panel $\{10^{-6}M_\odot, 10^{-4}\text{Hz}\}$. We also sampled $\{10^{-2}M_\odot, 1\text{Hz}\}$ and $\{10^{-4}M_\odot, 10^{-2}\text{Hz}\}$, and found almost identical results as for $\{10^{-6}M_\odot, 10^{-4}\text{Hz}\}$.

The choice of the parameter sets makes the observed frequency below the merger frequency of the IMR waveform at a redshift $z = 0$. We do not find a significant difference for C_l at different multipole l when choosing different f_H . The behavior of the C_l ratio at 100Hz is different from the other cases we studied ($\nu = 10^{-2}\text{Hz}$, 10^{-4}Hz , and 10^{-6}Hz), which is, in turn, similar to the behavior of C_l shown in Figure 5. There exists a turn-around frequency ν_{ta} for a given f_H and M_{PBH} or effectively M_c such that C_l decreases as ν increases when $\nu < \nu_{\text{ta}}$, while C_l increases when $\nu \geq \nu_{\text{ta}}$. Similarly, for a fixed observed frequency ν and multiple f_H and M_H or equivalently $M_{\text{PBH}, \text{max}} = 2.05M_H$, we can define a minimal turn-around frequency $\nu_{\text{ta}, \text{min}} = \min\{\nu_{\text{ta}}(M_{H,i} f_{H,i}^2)\}$ and a maximal turn-around frequency $\nu_{\text{ta}, \text{max}} = \max\{\nu_{\text{ta}}(M_{H,i} f_{H,i}^2)\}$. If $\nu < \nu_{\text{ta}, \text{min}}$, C_l will generally decrease as M_H increases. If $\nu > \nu_{\text{ta}, \text{max}}$, C_l will generally increase as M_H increases.

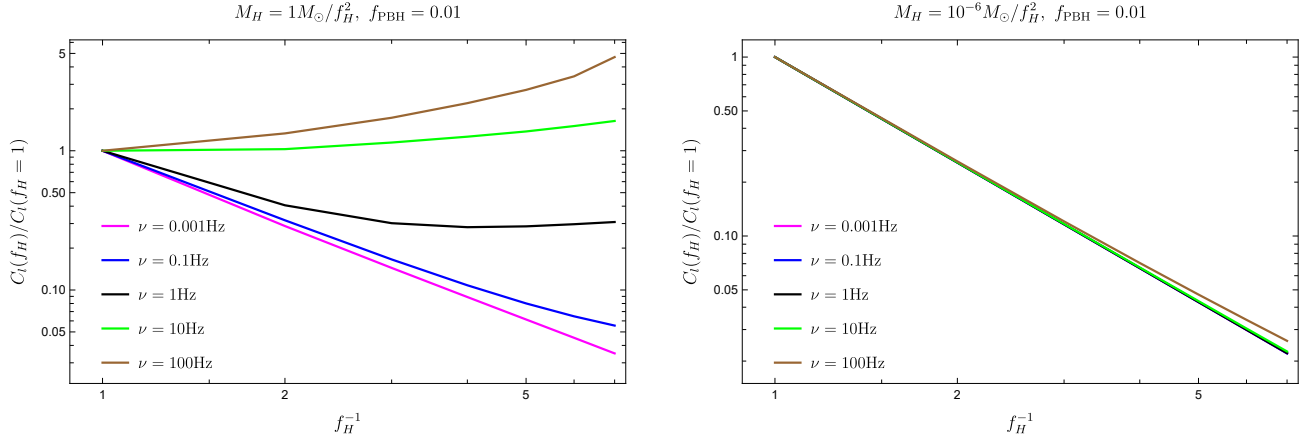


FIG. 9. The angular power spectra for $l = 1$ as a function of f_H^{-1} normalized by $C_l(\nu; f_H = 1)$ for different frequencies. The left panel is using $M_H = 1M_\odot/f_H^2$, while the right panel is using $M_H = 10^{-6}M_\odot/f_H^2$.

The ratio $C_l(f_H)/C_l(f_H = 1)$ is an f_H -dependent and frequency-dependent object, as shown in Figure 9. To analytically understand this behavior, we first rewrite $j_l(x)$ using the Limber approximation,

$$j_l(x) \approx \sqrt{\frac{\pi}{2l+1}} \delta(x - (l + 0.5)), \quad (32)$$

where $\delta(x)$ is the Dirac δ function. Applying the Limber approximation to Eq. 30 by replacing $x = k\Delta\eta = k(\eta - \eta_0)$, we can integrate the conformal time integral by using the Dirac δ -function, which gives

$$\delta_l(\nu, k) = \sqrt{\frac{\pi}{2l+1}} \frac{\nu}{\bar{\Omega}_{\text{gw}}(\nu)\rho_c} \frac{\mathcal{L}(\eta_*, \nu_s)}{1+z_*} \frac{\delta_{m,k}(\eta_*)}{k}, \quad (33)$$

where $\eta_* = \eta_0 - \frac{l+0.5}{k}$ is the conformal time determined by different sets of $\{l, k\}$ such that the argument of the Dirac δ -function in Eq. (32) is zero, and z_* is the redshift evaluated at η_* . The angular power spectrum is thus simplified in the following,

$$C_l(\nu) = \frac{2}{2l+1} \left(\frac{\nu}{\bar{\Omega}_{\text{gw}}(\nu)\rho_c} \right)^2 \int dk \frac{\mathcal{L}^2(\eta_*, \nu_s)}{(1+z_*)^2} \delta_{m,k}^2(\eta_*). \quad (34)$$

For a fixed l and a fixed observed frequency ν but different f_H , the ratio of C_l is given by,

$$\frac{C_l(\nu; f_H)}{C_l(\nu; f_H = 1)} = \left(\frac{\bar{\Omega}_{\text{gw}}(\nu; f_H = 1)}{\bar{\Omega}_{\text{gw}}(\nu; f_H)} \right)^2 \left(\frac{I(\nu; f_H)}{I(\nu; f_H = 1)} \right)^2, \quad (35)$$

where $I(\nu; f_H) = \int dk \frac{\mathcal{L}^2(\eta_*, \nu_s; f_H)}{(1+z_*)^2} \delta_{m,k}^2(\eta_*)$.

In the present scenario under consideration, the horizon mass is increased by a factor of f_H^{-2} when PBHs are formed in the radiation-dominated era, and thus the maximal PBH mass is also increased by the same factor. Note that in early matter domination, the horizon mass would also be increased, but by the smaller factor $f_H^{-3/2}$; in a general cosmology where the equation of state of the dominant species is $P = w\rho$, the horizon mass varies as $f_H^{-3(w+1)/2}$. The mass function also depends on f_H since the width of the distribution PDF(δ_1) depends on f_H , i.e., $\sigma_0 = \sigma_0(f_H)$ if A_s is given. Since PDF(δ_1) is a Gaussian distribution, the shape of the distribution is sensitive to the change in σ_0 . Therefore, the merger rate and the GW energy spectrum depend on f_H non-trivially in general. For example, the merger rate depends on the total mass of the binary system by $M_{\text{tot}}^{-32/37}$, in which we suppose the two BHs have the same mass, i.e., $\eta(m_1, m_2) = 0.25 = \eta_{\text{max}}$, but for different f_H the mass function is different, and it can peak at different $x = M_{\text{PBH}}/M_H$ (see Figure 2), so only using f_H cannot analytically predict the behavior of the merger rate. *However, by requiring a fixed f_{PBH} , the σ_0^2 is almost determined, and varying f_H only affects the horizon mass when PBHs form and PBH formation time.* For the GW energy spectrum, varying f_H will directly vary the spectrum amplitude – the spectrum amplitude is proportional to $M_{\text{tot}}^{5/3}$ if $m_1 = m_2$ for the inspiral phase where ν is smaller

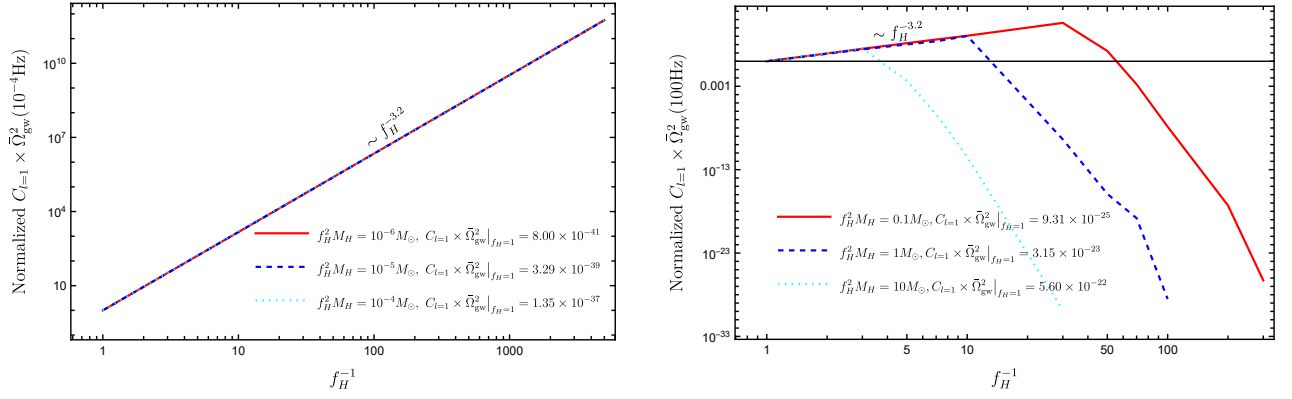


FIG. 10. The absolute value of angular power spectra as a function of f_H^{-1} at 10^{-4}Hz (left) and 100Hz (right) for $l = 1$ and different values of $f_H^2 M_H$ normalized by the corresponding $C_{l=1} \times \bar{\Omega}_{\text{gw}}^2|_{f_H=1}$, with $f_{H,\text{min}} = 5000^{-1}$ (left) and $f_{H,\text{min}} = 300^{-1}$ (right). The black solid line in the right panel indicates the value of 1.

than the merger frequency, and the shape of the spectrum, e.g., the cutoff frequency shifts to a lower frequency for a larger chirp mass M_c .

Even though σ_0^2 is highly suppressed at a large $f_H^{-1} \gtrsim 10$ for a given A_s , we further study the regime where $f_H^{-1} \gg 1$ for completeness, noting that this regime is also theoretically motivated by several deeply sub-horizon formation mechanisms [21, 22]. We note that since we require $f_{\text{PBH}} = 0.01$ in the plots, the value of σ_0^2 is almost unchanged even for large f_H^{-1} by manually tuning A_s . Figure 10 (left) shows the absolute angular power spectra $C_l \times \bar{\Omega}_{\text{gw}}$ of $l = 1$ and $f_{\text{PBH}} = 0.05$ as a function of f_H^{-1} at $\nu = 10^{-4}\text{Hz}$ and $f_H^2 M_H \in \{10^{-6}M_\odot, 10^{-5}M_\odot, 10^{-4}M_\odot\}$, while Figure 10 (right) shows the similar angular power spectra at $\nu = 100\text{Hz}$ and $f_H^2 M_H \in \{0.1M_\odot, 1M_\odot, 10M_\odot\}$. There is a manifest power-law behavior for the left subplot across the whole range of f_H^{-1} and for the right subplot right before the spectrum drops significantly due to the fact that the observed frequency is far above the cutoff frequency of the GW energy spectrum.

The f_H -dependence or effectively M_{PBH} -dependence of the absolute angular power spectrum can be understood as follows: First, when considering the observed frequency in the inspiral phase of the IMR spectrum and the two PBHs in the binary have the same mass, we notice the f_H -dependence of the isotropic SGWB energy density :

$$\bar{\Omega}_{\text{gw,inspiral}} \propto \mathcal{L} \propto \left. \frac{dE}{d\nu} \right|_{\text{inspiral}} \times \mathcal{R} \propto f_H^{-1.6}, \quad (36)$$

where the power law index, $1.6 \approx (\frac{5}{3} - \frac{32}{37}) \times 2$, is determined by the binary PBH mass dependence from both the merger rate and GW energy spectrum, i.e., $\mathcal{R} \propto M_b^{-32/37}$ and $\left. \frac{dE}{d\nu} \right|_{\text{inspiral}} \propto M_b^{5/3}$. By using the above power-law f_H -dependence, we can further show that the $C_l \times \bar{\Omega}_{\text{gw}}^2$ ratio (shown in Figure 10) has the power-law behavior with respect to f_H :

$$C_l \times \bar{\Omega}_{\text{gw}}^2(f_H) \propto \mathcal{L}^2 \propto \left(\left. \frac{dE}{d\nu} \right|_{\text{inspiral}} \times \mathcal{R} \right)^2 \propto f_H^{-3.2}, \quad (37)$$

where we have used the fact that f_H -dependence on C_l is sub-dominant compared to the one on $\bar{\Omega}_{\text{gw}}^2$, which can be found by considering the cancellation of f_H -dependence between $\bar{\Omega}_{\text{gw}}$ and \mathcal{L} in Eq. (35) and can be cross-checked by comparing Figure 8 and Figure 10 for $\nu = 100\text{Hz}$ and 10^{-4}Hz .

Finally, we show in Figure 11 the angular power spectra as a function of l given large values of $f_H^{-1} = 100, 700$, and 5000 at $\{\nu = 10^{-4}\text{Hz}, M_H = 10^{-6}M_\odot\}$ (left panel), and the corresponding ones for $f_H^{-1} = 10, 30$, and 100 at $\{\nu = 10\text{Hz}, M_H = 1M_\odot\}$ in Figure 11 (right panel). There is no unexpected behavior in the C_l ratio for different l except the case for $f_H^{-1} = 100$ in the right subplot. This is, again, because M_{PBH} increases with f_H^{-2} , and as a result the cutoff frequency of the IMR waveform shifts to a lower frequency which is far below the observed frequency.

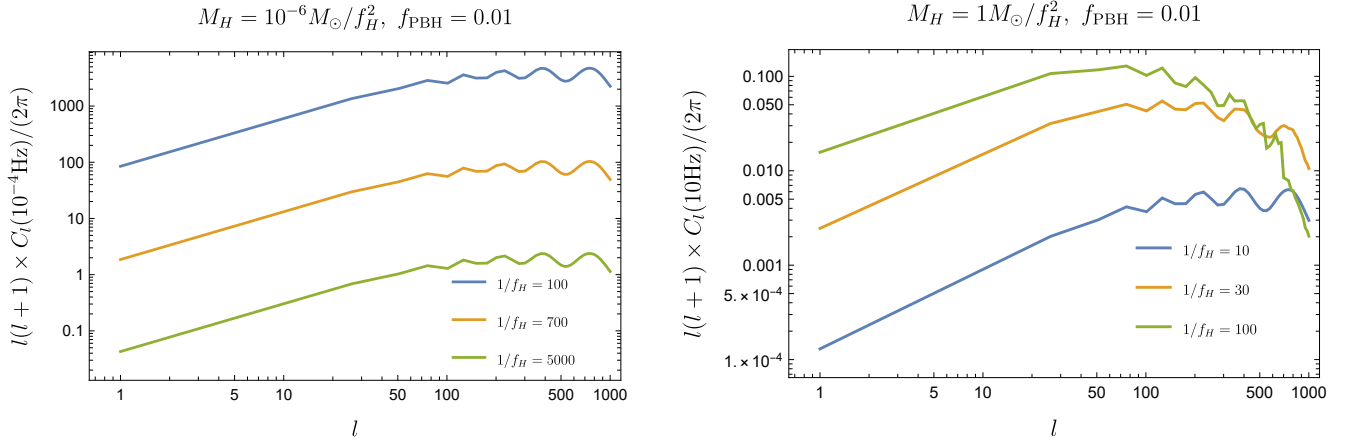


FIG. 11. The angular power spectra as a function of multipole l for $f_H^{-1} = 100, 700, 5000$ with $\{\nu = 10^{-4}\text{Hz}, M_H = 10^{-6}M_\odot\}$ (left) and for $f_H^{-1} = 10, 30, 100$ with $\{\nu = 10\text{Hz}, M_H = 1M_\odot\}$ (right).

IV. DISCUSSION AND CONCLUSION

We performed, for the first time, a comprehensive study of the behavior of the isotropic SGWB energy density spectrum and the angular power spectrum of PBH binary mergers for PBH forming from the collapse of sub-horizon patches. We introduced a model-independent parameter f_H characterizing the fraction of the wavelength of the perturbation mode in units of the horizon radius where the patch gravitationally collapses into a BH. The standard scenario is recovered for $f_H = 1$, whereas values $f_H < 1$ correspond to sub-horizon collapsing regions. We illustrated our findings using a simple Dirac- δ peak curvature spectrum, but the spectrum shape can be modified easily depending on the specific sub-horizon PBH formation mechanism. One of the limitations in our results is the assumption of a spherically symmetric distribution of overdensities, which in general can be non-spherically distributed when entering the regime of very small f_H .

We found that the sub-horizon PBH formation in general *enhances* the isotropic SGWB energy density $\bar{\Omega}_{\text{gw}}$ and the absolute angular power spectrum $C_l \times \bar{\Omega}_{\text{gw}}^2$. However, the almost monotonic increases in both $\bar{\Omega}_{\text{gw}}$ and $C_l \times \bar{\Omega}_{\text{gw}}^2$, as f_H decreases, cease when the chirp mass of binary PBHs reaches a mass threshold determined by a given observed frequency, such that the isotropic SGWB energy density spectrum significantly drops above that specific cutoff frequency. The important effect of the sub-horizon formation is changing the PBH mass (distribution) and also the formation time or redshift of PBHs, which in turn affects the GW observables, including both $\bar{\Omega}_{\text{gw}}$ and $C_l \times \bar{\Omega}_{\text{gw}}^2$.

We investigated the isotropic SGWB energy density spectrum and the angular power spectrum at various frequencies, PBH masses, and horizon size fractions f_H during PBH formation. When the observed frequency sits at the frequency range of the inspiral phase of the IMR waveform, the isotropic SGWB energy density spectrum and the absolute angular power spectrum at that frequency have f_H -dependent power-law behaviors, i.e., $\bar{\Omega}_{\text{gw}} \propto f_H^{-1.6}$ and $C_l \times \bar{\Omega}_{\text{gw}}^2 \propto f_H^{-3.2}$.

By introducing a sub-horizon formation scenario in the calculation of $\bar{\Omega}_{\text{gw}}$ and $C_l \times \bar{\Omega}_{\text{gw}}^2$, one can study the rich phenomenology of PBHs formed by non-standard mechanisms across the universe's history and provide a way to potentially test PBH formation mechanisms upon the hopefully forthcoming detection of an SGWB signal.

ACKNOWLEDGMENTS

This work is supported in part by the U.S. Department of Energy grant number de-sc0010107 (SP). F.W.Y. is supported by the U.S. Department of Energy under Award No. DESC0009959.

-
- [1] S. Hawking, Mon. Not. Roy. Astron. Soc. **152**, 75 (1971).
 - [2] B. Carr and F. Kuhnel, Ann. Rev. Nucl. Part. Sci. **70**, 355 (2020), arXiv:2006.02838 [astro-ph.CO].
 - [3] N. Smyth, L. Santos-Olmsted, and S. Profumo, JCAP **03**, 013 (2022), arXiv:2110.14660 [hep-ph].

- [4] L. Morrison, S. Profumo, and Y. Yu, JCAP **05**, 005 (2019), arXiv:1812.10606 [astro-ph.CO].
- [5] R. Bean and J. Magueijo, Phys. Rev. D **66**, 063505 (2002), arXiv:astro-ph/0204486.
- [6] S. Bird, I. Cholis, J. B. Muñoz, Y. Ali-Haïmoud, M. Kamionkowski, E. D. Kovetz, A. Raccanelli, and A. G. Riess, Phys. Rev. Lett. **116**, 201301 (2016), arXiv:1603.00464 [astro-ph.CO].
- [7] K. Belczynski, T. Bulik, C. L. Fryer, A. Ruiter, J. S. Vink, and J. R. Hurley, Astrophys. J. **714**, 1217 (2010), arXiv:0904.2784 [astro-ph.SR].
- [8] P. Giffin, J. Lloyd, S. D. McDermott, and S. Profumo, Phys. Rev. D **105**, 123030 (2022), arXiv:2105.06504 [hep-ph].
- [9] N. Fernandez and S. Profumo, JCAP **08**, 022 (2019), arXiv:1905.13019 [astro-ph.HE].
- [10] Z. Arzoumanian *et al.* (NANOGrav), Astrophys. J. Lett. **905**, L34 (2020), arXiv:2009.04496 [astro-ph.HE].
- [11] R. M. Shannon *et al.*, Science **349**, 1522 (2015), arXiv:1509.07320 [astro-ph.CO].
- [12] M. Raidal, V. Vaskonen, and H. Veermäe, JCAP **09**, 037 (2017), arXiv:1707.01480 [astro-ph.CO].
- [13] N. Bartolo, D. Bertacca, V. De Luca, G. Franciolini, S. Matarrese, M. Peloso, A. Ricciardone, A. Riotto, and G. Tasinato, JCAP **02**, 028 (2020), arXiv:1909.12619 [astro-ph.CO].
- [14] S. Wang, V. Vardanyan, and K. Kohri, Phys. Rev. D **106**, 123511 (2022), arXiv:2107.01935 [gr-qc].
- [15] S. S. Bavera, G. Franciolini, G. Cusin, A. Riotto, M. Zevin, and T. Fragos, Astron. Astrophys. **660**, A26 (2022), arXiv:2109.05836 [astro-ph.CO].
- [16] J. M. Bardeen, J. R. Bond, N. Kaiser, and A. S. Szalay, Astrophys. J. **304**, 15 (1986).
- [17] S. Young, I. Musco, and C. T. Byrnes, JCAP **11**, 012 (2019), arXiv:1904.00984 [astro-ph.CO].
- [18] I. Musco, Phys. Rev. D **100**, 123524 (2019), arXiv:1809.02127 [gr-qc].
- [19] S. Young, Int. J. Mod. Phys. D **29**, 2030002 (2019), arXiv:1905.01230 [astro-ph.CO].
- [20] T. Nakama, J. Silk, and M. Kamionkowski, Phys. Rev. D **95**, 043511 (2017), arXiv:1612.06264 [astro-ph.CO].
- [21] E. Cotner, A. Kusenko, M. Sasaki, and V. Takhistov, JCAP **10**, 077 (2019), arXiv:1907.10613 [astro-ph.CO].
- [22] S. W. Hawking, I. G. Moss, and J. M. Stewart, Phys. Rev. D **26**, 2681 (1982).
- [23] J. Garriga and A. Vilenkin, Phys. Rev. D **47**, 3265 (1993).
- [24] R. R. Caldwell and P. Casper, Phys. Rev. D **53**, 3002 (1996).
- [25] K. A. Meissner and H. Nicolai, Phys. Rev. D **102**, 103008 (2020), arXiv:2007.11889 [astro-ph.HE].
- [26] K. Kawana and K.-P. Xie, Phys. Lett. B **824**, 136791 (2022), arXiv:2106.00111 [astro-ph.CO].
- [27] M. M. Flores and A. Kusenko, Phys. Rev. Lett. **126**, 041101 (2021), arXiv:2008.12456 [astro-ph.CO].
- [28] A. Chakraborty, P. K. Chanda, K. L. Pandey, and S. Das, Astrophys. J. **932**, 119 (2022), arXiv:2204.09628 [astro-ph.CO].
- [29] J. F. Acevedo, J. Bramante, A. Goodman, J. Kopp, and T. Opferkuch, JCAP **04**, 026 (2021), arXiv:2012.09176 [hep-ph].
- [30] J. Abadie *et al.* (LIGO Scientific, VIRGO), Phys. Rev. D **83**, 122005 (2011), [Erratum: Phys.Rev.D 86, 069903 (2012)], arXiv:1102.3781 [gr-qc].
- [31] C. J. Moore, R. H. Cole, and C. P. L. Berry, Class. Quant. Grav. **32**, 015014 (2015), arXiv:1408.0740 [gr-qc].
- [32] B. Allen and J. D. Romano, Phys. Rev. D **59**, 102001 (1999), arXiv:gr-qc/9710117.
- [33] P. Ajith *et al.*, Phys. Rev. D **77**, 104017 (2008), [Erratum: Phys.Rev.D 79, 129901 (2009)], arXiv:0710.2335 [gr-qc].
- [34] P. Ajith *et al.*, Phys. Rev. Lett. **106**, 241101 (2011), arXiv:0909.2867 [gr-qc].
- [35] G. Cusin, C. Pitrou, and J.-P. Uzan, Phys. Rev. D **96**, 103019 (2017).
- [36] N. Aghanim *et al.* (Planck), Astron. Astrophys. **641**, A6 (2020), [Erratum: Astron.Astrophys. 652, C4 (2021)], arXiv:1807.06209 [astro-ph.CO].
- [37] M. Raidal, C. Spethmann, V. Vaskonen, and H. Veermäe, JCAP **02**, 018 (2019), arXiv:1812.01930 [astro-ph.CO].